P. Alvaredo, S. Tsipas, E. Gordo, Influence of carbon content on the sinterability of an FeCr matrix cermet reinforced with TiCN, *International Journal of Refractory Metals and Materials*, Jan. 2013, v. 36, 283-288, DOI: http://dx.doi.org/10.1016/j.ijrmhm.2012.10.007

Influence of carbon content on the sinterability of an FeCr matrix cermet reinforced with TiCN

P. Alvaredo, S. Tsipas, E. Gordo

palvared@ing.uc3m.es, stsipas@ing.uc3m.es, egordo@ing.uc3m.es

University Carlos III Madrid

Av. de la Universidad, 30 28911 Leganés (Spain)

Corresponding author: E. Gordo. (egordo@ing.uc3m.es)

University Carlos III Madrid

Av. de la Universidad, 30 28911 Leganés (Spain)

Telephone: +34 91 624 8862

Fax: +34 91 624 9430

Abstract

The influence of carbon content on an iron-chromium cermet composite reinforced with Ti(C,N) (50 vol%) has been studied. A thermodynamic simulation was performed using the ThermoCalc software to calculate the phase diagram of the composite. The results were validated by a thermal study performed using differential thermal analysis (DTA), and cermet samples with C percentages between 0 and 1 wt% added to the steel matrix were prepared using a conventional powder metallurgy process. The sintered samples were characterised by measurements of density and hardness, microstructural analysis using scanning electron microscopy (SEM), microanalyses using energy dispersive X ray spectroscopy (EDX) and X-ray diffraction (XRD). The results obtained show a significant influence of the C percentage on the solidus temperature, which influences sintering behaviour, leading to changes in the Ti(C,N) particles´ shape and composition, due to changes in the stoichiometry of the Ti(C,N). This influence is reflected in the cermet microstructure and hardness. The results are discussed with reference to the DTA and thermodynamic studies.

1. Introduction

Ti(C,N) -based cermets, with Ni and/or Co binders, are used increasingly in the cutting and forming industry, due to their high thermal and chemical stability and their excellent combination of hardness, oxidation resistance and toughness [1, 2]. However, the use of Co and Ni as metallic

matrixes presents health concerns due to the toxicity of these elements, which have been included in the lists of the International Agency for Research on Cancer (IARC). The elevated and fluctuating price of Co is also a concern [3].

For these reasons, there is growing interest in identifying alternative matrixes for cermets and cemented carbides. One of the most interesting candidates is Fe because of its lower price and toxicity and its ability to be hardened by heat treatment. In fact, Fe-based composite materials can be found on the market, commercialised as FerroTitanit® and FerroTiC®, which are composed of Fe alloys as a matrix and TiC as reinforcement, instead of Ti(C,N). The use of Ti(C,N) is preferred to TiC due to its greater hardness and strength, higher thermal conductivity and lower mass gain at high temperatures [6]. However, the use of Fe as a matrix makes processing more difficult because of the poor wettability of the liquid phase of Ti(C,N) particles during the sintering step. Some alloying elements and compounds, such as Cr, Mo, Mo_2C and W, have been reported to improve the wettability by decreasing the contact angle between the liquid matrix and the ceramic particles [7, 8], consequently improving the sinterability of the cermet. The carbon content also plays an important role in the sinterability and properties of Ti(C,N)-based cermets, as has been reported by some authors [9-11]. These studies are, however, related to Co- or Ni-based cermets; no studies are reported for Fe matrixes, although the phase transformations in steels are expected to have an influence. The study described in this paper was conducted to understand the combined influence of Cr and C on the sinterability, microstructure and properties of Fe- Ti(C,N) cermets. For this purpose, a prealloyed powder containing 16 wt% Cr, which corresponds to a commercially available 430L-grade stainless steel, was used as the matrix, and the carbon content was varied between 0 wt% and 1 wt%. The study includes a thermodynamic simulation of the Fe16Cr- Ti(C,N) system and validation of the results by experimental tests. Samples were produced by pressing and sintering, and a complete characterisation of the samples makes it possible to explain the differences found in the properties of the materials with different carbon contents.

2. Experimental Procedure

2.1 Fabrication of composite specimens

The matrix material used in this research was a prealloyed powder with a nominal composition of 16.2 wt% Cr, 0.75 wt% Si, 0.71 wt% Mn, and 0.026 wt% C, corresponding to stainless steel of grade 430L. Additional graphite (from ISTAM, ρ = 2.24 g/cm^3 and D50 = 18 µm) was added to the metallic matrix in the following amounts: 0.0, 0.25, 0.5, 0.75, and 1.0 wt% C with respect to the matrix weight. The reinforcement material was Ti(C,N), using a fixed amount of 50 vol% (equivalent to 40 wt%), so that the carbon content of the materials studied can be expressed as

[430+x wt% C]/ Ti(C,N) (where x is 0, 0.25, 0.5, 0.75, or 1.0). The characteristics of the starting powders are shown in Table 1.

Table 1. Characteristics of the raw materials, from supplier data and experimental data.

The starting powders were blended for 4 hours in a Turbula® multidirectional mixer to ensure complete homogenisation. The powders were then cold-pressed into rectangular bars (12x30x3 mm) at 700 MPa in a uniaxial die and sintered in a vacuum (10^{-4} mbar) at 1450 ºC for 60 minutes.

2.2 Thermodynamic simulation and thermal analysis

A thermodynamic study to calculate the phase equilibrium diagram for the cermet and the matrix was performed using the Thermocalc software in combination with the TCFE5 database [12] (Scientific Group Thermodata Europe).

The thermal behaviour of the cermets with different C contents was studied by differential thermal analysis (DTA) on green compacts, using a SETARAM device (SETSYS Evolution 16/18). The analyses were conducted in an Al_2O_3 crucible under an Ar (99.999 %) atmosphere up to 1700 °C. The heating and cooling rates for all of the specimens were 20 °C/min.

2.3 Characterisation and microstructural evolution

The sintered samples were characterised by measuring their density and hardness, as well as by studying their microstructural evolution using X-ray diffraction (XRD) and scanning electron microscopy (SEM). Density was measured using an Accupyc He Pycnometer, which makes it possible to calculate the closed porosity. Hardness was measured in polished cross sections of the samples using a 30 kg load and expressed on the Vickers scale (HV30). The microstructure was examined using a Philips XL-30 scanning electron microscope (SEM), coupled with an electron dispersive X-ray (EDX) system that enables the identification of elements present in the different phases of the specimens. Philips X´Pert equipment was used for the X-ray diffraction (XRD) analyses, performed for phase identification and crystalline analysis. From the X-ray diffraction spectra, the Ti(C,N) lattice parameter was calculated using Cohen´s method [13], which was chosen to avoid systematic measurement errors in the calculation of the lattice parameter from the diffraction angle [14].

3. Results and discussion

3.1. Thermodynamic calculation of the phase diagram

The phase diagrams shown in Figure 1 were calculated using the Thermocalc software. The diagram in Figure 1a corresponds to the composition of the 430L stainless steel (Fe16Cr) with respect to the carbon content. This diagram, obtained using the Thermocalc software, agrees well with Fe-Cr-C diagrams found in the literature [15]. The diagrams obtained using the Thermocalc software can therefore be considered good first approximations of the thermodynamic calculation of this material. The diagram in Figure 1b corresponds to the same steel with Ti(C,N) additions, calculated with the objective of determining the differences expected in the microstructure.

To calculate the equilibrium phase diagram shown in figure 1b, taking into account the presence of Ti(C,N) in the steel matrix, the elements Ti, C and N were introduced in the calculation in the mass percentages that correspond to a mixture containing 430/Ti(C,N) of 50 vol% each. The amount of C was varied considering the additional C added to the mixture (0.25 wt%, 0.5 wt%, 0.75 wt% and 1.0 wt% with respect to the weight of 430L). Considering all of the C present, including that from Ti(C,N), that from the 430L matrix and the additional C added, the total mass percentage of C varied between 3.99 wt% for the sample with no additional C and 4.62 wt% for the sample containing 1.0 wt% C added. The total percentage variation in C did not vary much because most of the C was due to the presence of Ti(C,N). The dotted vertical lines drawn in the diagram correspond to these percentages.

According to the phase diagram, the following phases appear to be stable in the different regions: ferrite, austenite, sigma, Ti(C,N) and carbides $M_{23}C_6$ and M_7C_3. The phase diagram indicates the presence of the Ti(C,N) phase with mass percentages corresponding to the stoichiometry of approximately $Ti(C_{0.5}N_{0.5})$ in most of the phase fields, which is an indicator that the phase diagram is a good first attempt at representing the system 430L/Ti(C,N) because Ti(C,N) was not introduced as a compound in the calculation, and only the individual elements Ti, C and N, in the amounts present in the mixture, were introduced. Therefore, even though the equilibrium phase diagram remains a first approximation, it can still be considered valid for the present discussion.

Figure 1 Equilibrium phase diagram for a material with a composition of (a) 430L stainless steel, and (b) 430L + Ti(C,N) 50 vol% as a function of C content (wt%).

Some important aspects of the phase diagram to consider that will be discussed later in view of the properties of the cermet materials are the following: (1) the solidus temperature appears to be lower in the phase diagram for the case when Ti(C,N) is considered (Figure 1b) compared to the solidus temperature in the 430L phase diagram (Figure 1a); (2) the solidus temperature decreases with increasing C content in the steel matrix in both phase diagrams; (3) at room temperature (considering that the phases found at room temperature are the same as those at 500 °C), in samples with no additional C addition and with 0.25 wt% C added, the σ phase is formed; and (4)

carbide $M_{23}C_6$ is found at room temperature for all of the compositions, but carbide M_7C_3 is formed only in the sample with 1 wt% of added C.

3.2 Differential thermal analysis (DTA)

Figure 2 shows the heating range of the DTA curves for mixtures of 430L matrix and TiCN with different carbon additions up to temperatures of 1700ºC, as well as the DTA curve for the 430L steel matrix without any reinforcement. The curve corresponding to the 430L steel matrix without reinforcement shows only one peak at 1518 °C, corresponding to the melting point, which agrees quite well with values reported in the literature. This temperature is also in accordance with the liquidus temperature obtained (1506 °C) in the stainless steel phase diagram calculated using the Thermocalc software (Figure 1a). When Ti(C,N) is added to the 430 matrix, the superposition of two peaks can be distinguished, and they appear at a lower temperature than they do for plain 430L. As the carbon content increases, these two peaks become more defined and further apart, and in the materials with the highest carbon content (0.75 wt% and 1 wt%), the emergence of a third peak is observed.

Figure 2 Comparison of DTA heating curves of mixtures [430+x wt% C]/ Ti(C,N) (x = 0, 0.25, 0.5, 0.75, 1.0) and 430L stainless steel.

Figure 3 shows the cooling range of the DTA curves, where all of the peaks are exothermic. The curve corresponding to the plain stainless steel shows only one peak at a lower temperature than the endothermic peak in the heating curve. In the curve corresponding to the cermet 430/ Ti(C,N) without C added, again, the superposition of two peaks appears, as well as in the curve for the sample with 0.25 wt%. The DTA curves for the samples with higher C amounts exhibit a third peak. The appearance of the same peaks in the heating and cooling curves indicates that those peaks correspond with reversible reactions, such as melting and solidification of species or phase transformations.

Figure 3 Comparison of DTA cooling curves of mixtures [430+x wt% C]/ Ti(C,N) (x = 0, 0.25, 0.5, 0.75, 1.0) and 430L stainless steel.

Interpreting the DTA measurements with the aid of the calculated phase diagrams, the following observations can be made. The solidus and liquidus temperatures of the stainless steel decrease with increasing carbon content, and the difference between these two temperatures increases with increasing carbon content. In Figure 4, the solidus and liquidus temperatures calculated using the

Thermocalc phase diagram of the cermet are shown with respect to the C content. The difference between the two temperatures with no C addition is 45 ºC. Such a difference is too small to be distinguished by two distinct peaks in the DTA measurement; hence, the two peaks appear to be superimposed. This is in accordance with the DTA curve for the sample 430/ Ti(C,N) (Figure 2), where the superposition of two peaks can be distinguished.

Figure 4 Liquidus and solidus temperatures of the cermet 430/ Ti(C,N) with respect to the C content calculated from the Thermocalc phase diagram.

For 0.25 % and 0.5 % added C, the difference between the solidus and liquidus temperatures in the phase diagram is approximately 65 ºC, and some changes are observed in the DTA curve. The two peaks become more defined, possibly because DTA measurement can detect both temperatures because of this wider region in the diagram. Nevertheless, examining both the heating and cooling curves (Figure 2 and Figure 3), the cooling curves of both materials show two peaks, one of which is wider. Examining the solid state transformations represented in the phase diagram for these compositions closely, it appears possible that the wider peak could itself be due to the superposition of two separate peaks, one corresponding to the solidus temperature and the second corresponding to the transformation of α to γ.

In the DTA curves of the samples with higher C percentages, 0.75 %C and 1.0 %C, three peaks can clearly be distinguished, one at approximately 1380 ºC, the second at 1400 ºC and the third at approximately 1500 ºC. These peaks could correspond to the liquidus temperature, the solidus temperature and the α→γ transformation. However, for these compositions, the temperatures for the transitions observed in the DTA curves are not in accordance with the transition temperatures observed in the calculated phase diagram.

Although the Thermocalc phase diagram could be a very good first approximation at describing the high-temperature behaviour of this system, the phase diagram does not accurately represent the experimental system. The software takes into account the equilibrium stoichiometric composition of Ti(C,N), namely, $Ti(C_{0.5}N_{0.5})$, in the calculation of the phase diagram. Nevertheless, as will be explained in the following section in more detail, during sintering, the stoichiometry of this compound could change. Hence, the amount of C and N available would be affected, and this would modify the phase diagram and subsequently the liquidus and solidus temperatures. As a result, the regions shown in the diagram differ in terms of C percentage. This could explain possible discrepancies between the temperatures of phase transitions in the calculated phase diagrams and the DTA experiments.

3.3 Characterisation of sintered samples

The microstructures of the sintered samples with different C amounts are shown in Figure 5. Two distinct phases are visible. The grey phase corresponds to the stainless steel matrix, and the black phase corresponds to the Ti(C,N) particles. At first glance, the microstructures of the cermets with increasing C amount appear to be quite similar and do not show remarkable differences. Only the stainless steel matrix of the sample with 1 wt% C shows two different tones, due to the presence of the M_3C_7, the formation of which was predicted in the phase diagram. In addition, examining all of the microstructures carefully, it is possible to observe that the samples without C or with low amounts of C have a more heterogeneous microstructure, while the sample with 0.5 wt% C has a clean and homogeneous microstructure. These differences in the microstructure could be explained in terms of the different thermal behaviours of mixtures of 430/Ti(C,N) with different C percentages, taking into account the characteristic sintering mechanism of Ti(C,N)-based cermets [16].

Ti(C,N)-based cermets are sintered by liquid-phase sintering, and the mechanism involves a dissolution-precipitation process. During liquid-phase sintering, the metallic matrix dissolves some of the Ti(C,N) particles, which reprecipitate again during cooling [18]. As seen previously, increasing the C content decreases the liquidus temperature of the stainless steel; therefore, each cermet will exhibit a different sintering mechanism, which will be reflected in its microstructure, especially in terms of Ti(C,N) particle shape and composition.

Ti(C,N) is a compound with an FCC NaCl-type structure, with C and N atoms situated randomly in octahedral sites [17]. The dissolution and reprecipitation of Ti(C,N) particles during sintering results in dissolution of C or N from the Ti(C,N) structure toward the metallic matrix. This causes changes in the stoichiometry and composition of the Ti(C,N) particles, which are reflected in changes in the Ti(C,N) lattice parameter.

Figure 5 SEM microstructures of [430 + x wt% C]/ Ti(C,N) (x = 0, 0.25, 0.5, 0.75, 1.0) samples sintered at 1450 °C for 60 minutes in a vacuum.

Figure 6 shows XRD analyses of the [430 + x %wt C]/ Ti(C,N) (x = 0, 0.25, 0.5, 0.75, 1.0) sintered samples. These analyses do not demonstrate any difference in the phases present in materials with different amounts of C. All of the XRD diffractograms exhibit peaks that correspond to ferrite and Ti(C,N), while no peaks corresponding to a sigma phase or carbides are visible, most likely because if they are present, they constitute a relative low percentage in the samples. Although no differences in the phases formed were detected in the XRD analysis, there is a displacement of the diffraction angle of the peaks corresponding to the Ti(C,N) phase, depending on the carbon content of the samples. This displacement is associated with changes in the Ti(C,N) stoichiometry due to its dissolution during the sintering process, which is reflected in the change of the Ti(C,N) lattice parameter with increasing C content.

Figure 6 XRD analysis of [430 + x wt% C]/ Ti(C,N) (x = 0, 0.25, 0.5, 0.75, 1.0) sintered samples.

Figure 7 shows the lattice parameter of [430 + x wt% C]/Ti(C,N) (x = 0, 0.25, 0.5, 0.75, 1.0) sintered samples calculated from the angle of diffraction obtained from XRD analysis. For comparison, the lattice parameter of the Ti($C_{0.5}N_{0.5}$) starting powder, obtained prior to mixture with the metallic matrix and fabrication of the sintered samples, is also plotted. The lattice parameter of the samples with 0 and 0.25 wt% C is lower than the lattice parameter of the starting powder of Ti($C_{0.5}N_{0.5}$), which was found to be 4.2855 Å. This is most likely due to dissolution of C from Ti(C,N) particles toward the metallic matrix during sintering, as mentioned earlier. The lattice parameter of the sample with 0.5 %wt C is quite similar to the lattice parameter of the starting powders, which suggests a slight change in the Ti(C,N) particles during sintering. This agrees quite well with the observations of the microstructure of this sample, which exhibits Ti(C,N) particles with cubic shape. The lattice parameter of the sample with 0.75 wt% C exhibits the highest value, whereas an increase in the percentage of C to 1 wt% corresponds to a decrease in the lattice parameter to its lowest value observed in this study, 4.2708 Å. An increase in the lattice parameter for 0.75 wt% C could be due to dissolution of C from the metallic matrix toward Ti(C,N) particles, due to an excess of C in the matrix. However, when the carbon content is increased to 1 wt%, according to the phase diagram, the C content is now sufficient for the formation of M_7C_3 carbide. Therefore, that carbon is consumed in the formation of this carbide, and there is no excess of C in the metallic matrix. As a result, the stoichiometry of Ti(C,N) changes (it now contains less C) due to the formation of the carbide M_7C_3.

Figure 7 Lattice parameter of Ti(C,N) particles in [430 + x %wt C]/TiCN (x = 0, 0.25, 0.5, 0.75, 1.0) sintered samples and lattice parameter of TiCN starting powder.

In Figure 8, the values of the hardness and relative density of the sintered samples of the cermets with increasing C amounts are represented. These values are a reflection of their thermal behaviour, microstructures and composition. The highest relative densities are achieved in the samples with higher C contents, due to their lower liquidus temperature, which implies better densification during sintering. The samples containing 0 and 0.25 wt% C exhibit the lowest hardness values, most likely due to the presence of a sigma phase and their heterogeneous microstructure. The highest hardness is measured for the sample with 0.5 wt% C, due to its homogeneous microstructure. The lowest hardness is measured for the sample with 1 wt%, most likely due to the presence of M_7C_3 carbide.

Figure 8 Relative density and hardness of [430 + x %wt C]/ Ti(C,N) (x = 0, 0.25, 0.5, 0.75, 1.0) sintered samples

4. Conclusions

In this paper, the influence of carbon content on the thermodynamic and thermal behaviour of sintered samples of a stainless steel matrix cermet was investigated. The main conclusions are the following:

- Thermodynamic calculations and data from thermal analysis of the samples show good agreement. The combination of the two techniques is helpful in understanding the differences observed among sintered samples with different C contents.
- Due to the nature of the sintering mechanism of Ti(C,N)-based cermets, dissolution and reprecipitation of Ti(C,N) particles, the composition and shape of the reinforcement is influenced by the thermal behaviour of the sample.
- The hardest sample was the one containing 0.5 wt% C. This sample had a homogenous microstructure with cubic Ti(C,N) particles, and its lattice parameter was quite similar to the lattice parameter of the starting powder.

5. Acknowledgements

The authors would like to acknowledge the financial support of the Spanish Ministry of Science and Innovation through R&D Project MAT2009-14448-C02 and the Regional Government of Madrid through the program ESTRUMAT-CM (Ref. S2009/MAT-1585).

6. References

[1] Pastor H. Titanium-carbonitride-based hard alloys for cutting tools. Adv. Mater. Sci. Eng. 1988;105-106:401-9.

[2] Ettmayer P, Kolaska H, Lengauer W, Dreyer K. Ti(C,N) cermets -- Metallurgy and properties. Int. J. Refract. Met. Hard Mater 1995;13:343-51.

[3] B. Gries LP. Acute inhalation toxicity by contact corrosion - the case of WC-Co. In: EPMA, editor. Proceedings EURO PM2007 Shrewsbury2007. p. 189-96.

[4] Gruss WW. Cermets. Metals Handbook. 9th ed: ASM International; 1989. p. 90-7.

[5] Zhou SQ, Zhao W, Xiong WH, Zhou YN. Effect of Mo and Mo2C on the microstructure and properties of the cermets based on Ti(C,N). Acta Metall. Sinica 2008;21:211-9.
[6] Umanskii AP. Titanium carbonitride composite with iron chromium binder. Powder Metall. Met. Ceram. 2001;40:637-40.
[7] Li Y, Liu N, Zhang X, Rong C. Effect of carbon content on the microstructure and mechanical properties of ultra-fine grade (Ti,W) (C,N)-Co cermets. J. Mater. Process. Technol. 2008;206:365-73.
[8] Liu N, Liu X, Zhang X, Zhu L. Effect of carbon content on the microstructure and mechanical properties of superfine Ti(C, N)-based cermets. Mater. Charact. 2008;59:1440-6.
[9] Zackrisson J, Andrén HO. Effect of carbon content on the microstructure and mechanical properties of (Ti, W, Ta, Mo)(C, N)-(Co, Ni) cermets. Int. J. Refract. Met. Hard Mater 1999;17:265-73.
[10] Andersson JO, Helander T, Höglund L, Shi P, Sundman B. Thermo-Calc & DICTRA, computational tools for materials science. Calphad. 2002;26:273-312.
[11] Cullity BD. Elements of X-Ray diffraction. Addison-Wesley Publishing Company, Inc.; 1956.
[12] Sánchez JM, Alvarez M, Rodriguez N, Aristizabal M. Effect of Ni powder characteristics on the consolidation of ultrafine TiMoCN cermets by means of SPS and HIP technologies. Mater. Sci. Eng., A 2009;500:225-32.
[13] Roberts G. A., Kennedy R. L. Tool Steels. 5th ed: ASM International 1998. p. 63.
[14] Alvaredo P, Gordo E, Van der Biest O, Vanmeensel K. Microstructural development and mechanical properties of iron based cermets processed by pressureless and spark plasma sintering. Mater. Sci. Eng., A 2012;538:28-34.
[15] Andrén H-O. Microstructure development during sintering and heat-treatment of cemented carbides and cermets. Mater. Chem. Phys. 2001;67:209-13.
[16] Levi G, Kaplan WD, Bamberger M. Structure refinement of titanium carbonitride (TiCN). Mater. Lett. 1998;35:344-50.

Table(s)

Table 1. Characteristics of the raw materials, from supplier data and experimental data.

Raw material	Supplier	Supplier data		Experimental data	
		Density (g/cm^3)	Particle size (µm)	Density (g/cm^3)	Particle size (µm)
Ti(C,N)	H. C. Starck	5.03	D50 = 2.0–4.0	5.12	D50 = 4.6 D90 = 9.3
Stainless Steel 430L	Osprey	7.50	D90 < 16	7.70	D50 = 8.5 D90 = 16.2

Figure(s)

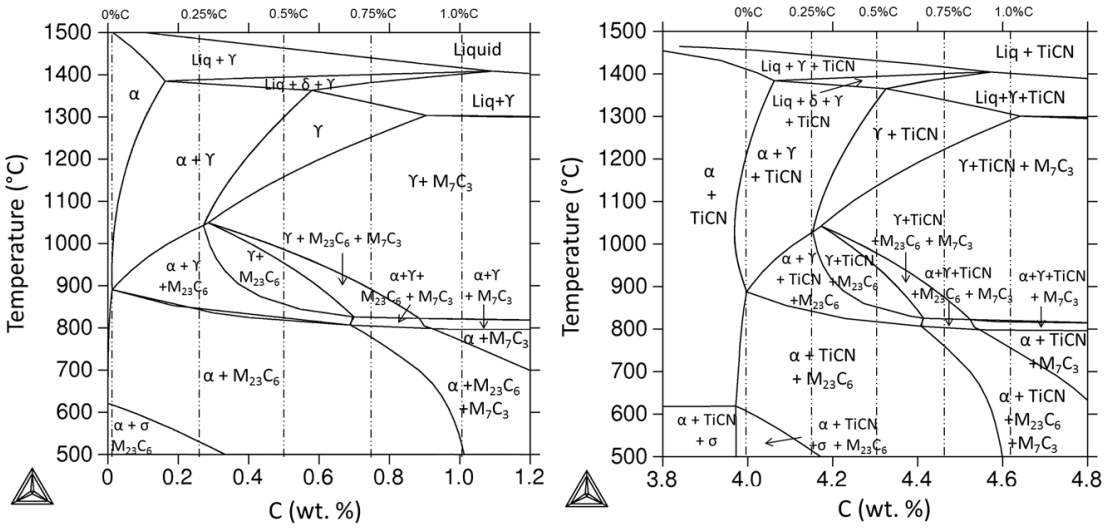

Figure 1 Equilibrium phase diagram for a material with a composition of (a) 430 stainless steel, and (b) 430 + Ti(C,N) 50 vol%, as a function of C content (wt %).

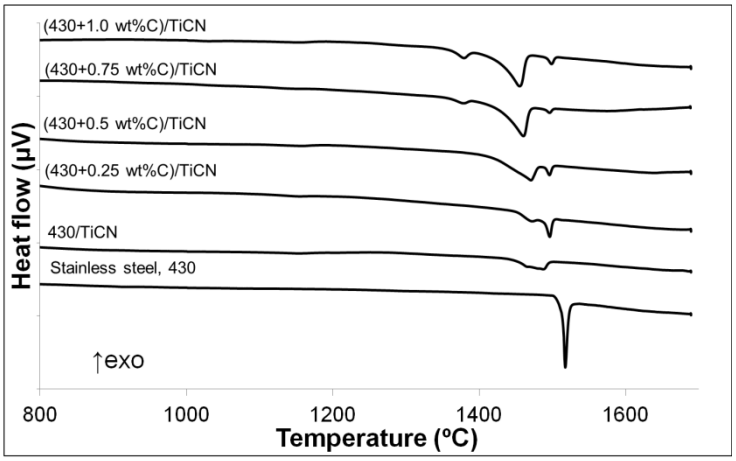

Figure 2 Comparison of DTA heating curves of mixtures [430+x wt% C]+Ti(C,N) (x = 0; 0.25; 0.5; 0.75; 1.0) and 430 stainless steel.

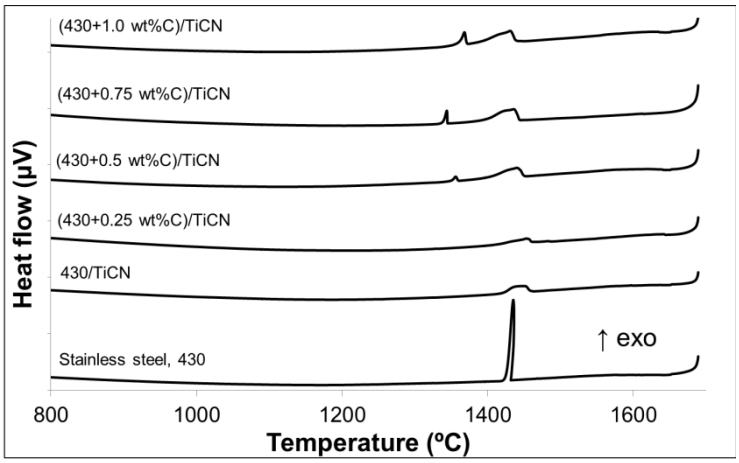

Figure 3 Comparison of DTA cooling curves of mixtures [430+x wt% C]+Ti(C,N) (x = 0; 0.25; 0.5; 0.75; 1.0) and 430 stainless steel.

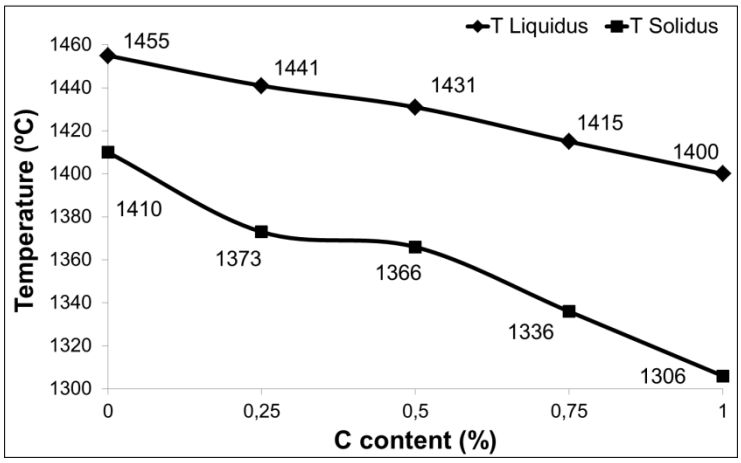

Figure 4 Liquidus and solidus temperatures of the cermet 430/Ti(C,N) with respect to the C content calculated from the Thermocalc phase diagram.

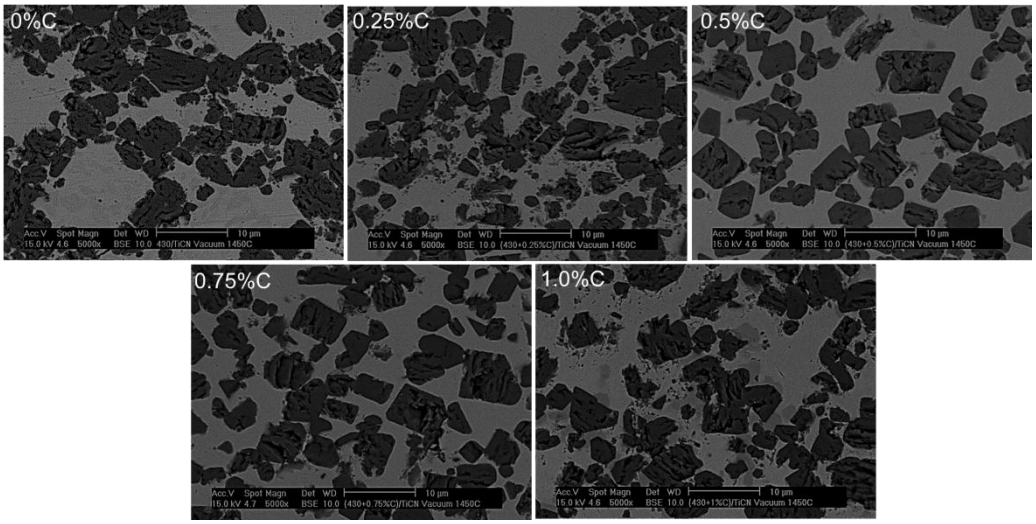

Figure 5 SEM microstructures of [430 + x wt% C]/Ti(C,N) (x = 0; 0.25; 0.5; 0.75; 1.0) samples sintered at 1450°C during 60 minutes under vacuum.

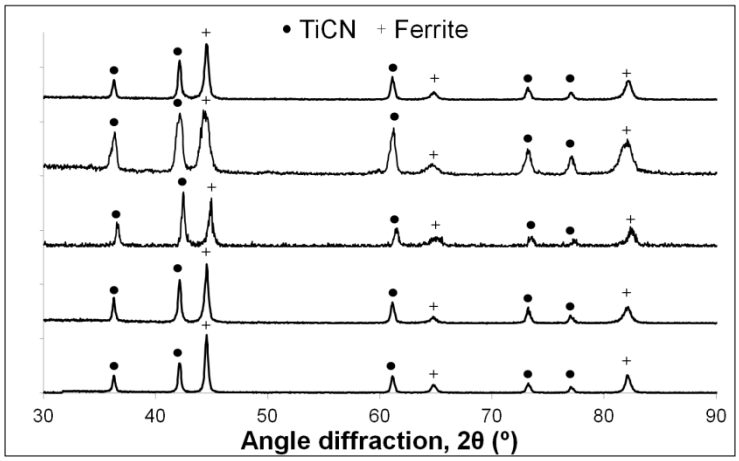

Figure 6 XRD analysis of [430 + xwt%. C]/Ti(C,N) (x = 0; 0.25; 0.5; 0.75; 1.0) sintered samples

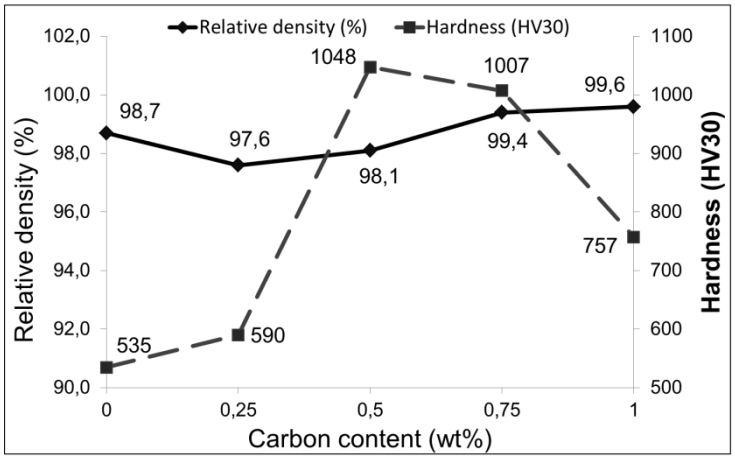

Figure 7 Lattice parameter of TiCN particles in [430 + x%wt. C]/Ti(C,N) (x = 0; 0.25; 0.5; 0.75; 1.0) sintered samples and lattice parameter of Ti(C,N) starting powder.

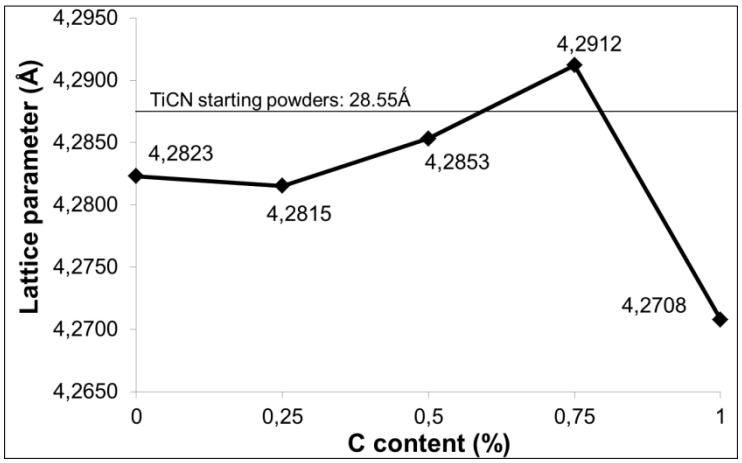

Figure 8 Relative density and hardness of [430 + x%wt. C]/Ti(C,N) (x = 0; 0.25; 0.5; 0.75; 1.0) sintered samples.